



Publication Year	2021
Acceptance in OA@INAF	2021-09-27T07:44:29Z
Title	γ Observations of the 3 -ray-emitting narrow-line Seyfert host galaxy
Authors	Timothy S. Hamilton; Marco Berton; Sonia Ant3n; BUSONI, LORENZO; CACCIANIGA, Alessandro; et al.
DOI	10.1093/mnras/stab1046
Handle	http://hdl.handle.net/20.500.12386/31050
Journal	MONTHLY NOTICES OF THE ROYAL ASTRONOMICAL SOCIETY
Number	504

Observations of the gamma-ray emitting narrow-line Seyfert 1, SBS 0846+513, and its host galaxy

Timothy S. Hamilton,^{1*} Marco Berton,^{2,3} Sonia Antón,^{4,5} Lorenzo Busoni,⁶ Alessandro Caccianiga,⁷ Stefano Ciroi,⁸ Wolfgang Gässler,⁹ Iskren Georgiev,⁹ Emilia Järvelä,¹⁰ S. Komossa,¹¹ Smita Mathur,¹² Sebastian Rabien¹³

¹*Department of Natural Sciences, Shawnee State University, 940 2nd St., Portsmouth, OH 45662, USA*

²*Finnish Centre for Astronomy with ESO (FINCA), University of Turku, Quantum, Vesilinnantie 5, FI-20014 University of Turku, Finland*

³*Aalto University Metsähovi Radio Observatory, Metsähovintie 114, FI-02540 Kylmälä, Finland*

⁴*CIDMA, Departamento de Física, Universidade de Aveiro, Campus Universitário de Santiago, 3810-193 Aveiro, Portugal*

⁵*Instituto de Telecomunicações, Campus Universitário, 3810-193 Aveiro, Portugal*

⁶*Arcetri Astrophysical Observatory, Largo Enrico Fermi 5, I-50125 Florence, Italy*

⁷*INAF - Osservatorio Astronomico di Brera, Via Brera 28, 20121 Milano, Italy*

⁸*Department of Physics and Astronomy, Padova University, Vicolo dell'Osservatorio 3, I-35122 Padova, Italy*

⁹*Max-Planck Institut für Astronomie, Königstuhl 17, D-69117 Heidelberg, Germany*

¹⁰*European Space Agency, European Space Astronomy Centre, C/ Bajo el Castillo s/n, 28692 Villanueva de la Cañada, Madrid, Spain*

¹¹*Max-Planck-Institut für Radioastronomie, Auf dem Hügel 69, D-53121 Bonn, Germany*

¹²*Department of Astronomy, The Ohio State University, 140 West 18th Avenue, Columbus, OH 43210, USA;*

Center for Cosmology and AstroParticle Physics, The Ohio State University, 191 West Woodruff Avenue, Columbus, OH 43210, USA

¹³*Max-Planck Institut für Extraterrestrische Physik, Giessenbachstrasse 1, D-85748 Garching, Germany*

Accepted XXX. Received YYY; in original form ZZZ

ABSTRACT

The gamma-ray emitting galaxy SBS 0846 + 513 has been classified as a Narrow-Line Seyfert 1 from its spectroscopy, and on that basis it was thought likely to have a small central black hole hosted in a spiral galaxy. But very few of the gamma-ray Narrow-Line Seyfert 1s have high-resolution imaging of their hosts, so it is unknown how those expectations hold up for the gamma-emitting class. We have observed this galaxy in the *J*-band with the Large Binocular Telescope's LUCI1 camera and the ARGOS adaptive optics system. We estimate its black hole mass to lie between $7.70 \leq \log \frac{M}{M_{\odot}} \leq 8.19$, using the correlation with bulge luminosity, or $7.96 \leq \log \frac{M}{M_{\odot}} \leq 8.16$ using the correlation with Sérsic index, putting its mass at the high end of the Narrow Line Seyfert 1 range. These estimates are independent of the Broad Line Region viewing geometry and avoid underestimates due to looking down the jet axis. Its host shows evidence of a bulge + disc structure, both from two-dimensional modeling and isophote shape, in keeping with the expectations. Mergers and interactions appear to be common among the gamma-ray Narrow-Line Seyfert 1s, and we see some circumstantial evidence for companion galaxies or disturbed features in the host.

Key words: instrumentation: adaptive optics – galaxies: active – galaxies: Seyfert – quasars: supermassive black holes

1 INTRODUCTION

The relation that links galaxies with the black hole (BH) at their centres has been known for a while, and it is valid for non-active and active galaxies (e.g., Ferrarese & Merritt 2000). The host galaxy of an active galactic nucleus (AGN) is the closest environment with which the nucleus interacts and co-evolves (Kormendy & Ho 2013). For example, accretion on to the central BH can ionize and heat the gas, suppressing the star formation (SF) in the circumnuclear region (Page et al. 2012). Simultaneously, the host directly affects the nuclear activity by regulating the gas supply of the BH. A remarkable example of this feedback is the interplay between the host and the relativistic plasma jet that can be launched by the BH. For example, jets are observed digging their way through the host galaxy gas (Morganti et

al. 2015), and they can efficiently suppress the SF activity far from the nucleus (Lanz et al. 2016). Although jets are crucial components in some AGN, they are far from understood. Why and how they are formed is still unclear, but the host galaxy likely plays a crucial role in this. In particular, powerful relativistic jets are preferentially, though not exclusively, associated with ellipticals (Laor 2000), and merging or interaction may be the keys that trigger the jet activity (Chiaberge et al. 2015).

An important new laboratory to study the jet phenomenon is the AGN class known as narrow-line Seyfert 1 (NLS1s). Many of the sources referred to as Narrow-Line Seyfert 1s are actually quasars under the standard definition (total magnitude $M < -23$), though this limit does not distinguish between the host and nuclear emission. The physical arguments regarding the Narrow-Line Seyfert 1s we expect to apply to narrow-line type-1 quasars, as well, and in this discussion, we refer to them collectively as NLS1. These objects

* E-mail: thamilton@shawnee.edu

were first classified by [Osterbrock & Pogge \(1985\)](#) and are defined by the low full width at half maximum of $H\beta$ ($< 2000 \text{ km s}^{-1}$; [Goodrich 1989](#)). The narrowness of permitted lines is believed to be due to the low rotational velocity around a low-mass black hole ($< 10^8 M_{\odot}$; [Grupe & Mathur 2004](#)). Other lines of reasoning support the idea of small BH masses for NLS1, including their X-ray power spectrum distribution ([Pan et al. 2018](#)) and the rapidity of their X-ray variability ([Boller et al. 1997](#); [Brandt et al. 1999](#); [Yao et al. 2015](#); [Gallo 2018](#)). Taking into account their luminosity, comparable to that of broad-line Seyfert 1s, this is suggestive of a high Eddington ratio ([Boroson & Green 1992](#)). These properties have been interpreted as a sign of young age ([Mathur 2000](#)). If this is the case, NLS1s may be the low- z analog of the progenitors of high-mass AGN, sharing properties with early quasars.

However, it has been claimed that NLS1s are not genuinely young AGN (e.g., [Sbarrato et al. 2018](#)). Narrow permitted lines may also be due to the projection effects caused by a flattened broad-line region observed pole-on ([Decarli et al. 2008](#)). Were this the case, the BH masses derived from spectral line widths ([Calderone et al. 2013](#)) would be underestimated. Fortunately, the host galaxy can help disentangling these two scenarios. Generally speaking, ellipticals tend to harbor more massive BH than spirals (e.g., [Salucci et al. 2000](#)), and the black hole mass correlates with properties of the bulge (e.g., [Magorrian et al. 1998](#); [Marconi & Hunt 2003](#); [Graham & Driver 2007](#)). So a measurement of the host galaxy type can tell us about the central black hole’s mass in a way that is independent of geometry.

In 2009, γ -rays were detected from radio-loud NLS1 ([Abdo et al. 2009](#)), and in the years since, about 19 NLS1 have been detected with the *Fermi Gamma-Ray Space Telescope* ([Romano et al. 2018](#); [Järvelä et al. 2020](#)). These have shown unambiguously that there exists a subset of NLS1 that are radio-loud and have powerful, relativistic jets, even though with their smaller black holes, they may have been expected not to ([Laor 2000](#)). The γ -NLS1s are an intriguing and still poorly-understood sample. If they are from the same broader population as the radio-quiet NLS1, then what triggers the relativistic jet? As described by [Komossa \(2018\)](#), a large number of γ -NLS1 seem to be in interacting systems. In fact, of the sources analysed in the study, only PKS 2004 – 447 and SBS 0846 + 513 did not show evidence for interaction at the then-available resolution. On the other hand, the majority of radio-quiet NLS1 do not show an excess of companion galaxies or evidence for mergers ([Krongold, Dultzin-Hacyan, & Marziani 2001](#); [Xu et al. 2012](#)). In general, jetted NLS1 preferably reside in denser regions than do the non-jetted NLS1 sources, at least in terms of large-scale environment ([Järvelä, Lähteenmäki, & Berton 2018](#)).

Perhaps the host galaxies are different between the radio-quiet NLS1 and the radio-loud (especially the γ -emitters). But only a few studies have been dedicated to the hosts of NLS1s. [Crenshaw, Kraemer, & Gabel \(2003\)](#) studied 19 NLS1s with HST, all non-jetted at $z < 0.084$, finding a majority of spirals and frequent starburst rings. A high incidence of pseudobulges was found by [Orban de Xivry et al. \(2011\)](#) and confirmed by a subsequent study with HST of 10 more non-jetted sources up to $z = 0.164$ ([Mathur et al. 2012](#)). However, nothing can be said for non-jetted sources at higher z . Regarding radio-loud, jetted NLS1s (~ 7 per cent of the whole NLS1 population; see [Komossa et al. 2006](#)), four sources have been studied individually ([Zhou et al. 2007](#); [Antón, Browne, & Marchā 2008](#); [Kotilainen et al. 2016](#); [Olguín-Iglesias et al. 2017](#); [D’Ammando et al. 2017, 2018](#); [Berton et al. 2019](#)). On a larger sample is that by [Järvelä, Lähteenmäki, & Berton \(2018\)](#) with the Nordic Optical Telescope (NOT), but even in that case only three jetted sources were successfully re-

solved. In general, the results are still unclear. Most jetted NLS1s studied so far are hosted by spirals and disturbed morphologies. The recent study by [Olguín-Iglesias, Kotilainen, & Chavushyan \(2020\)](#) further supports this result. They image 29 radio-loud NLS1s, successfully detecting 21 and fitting bulge + disc models. However, a couple of NLS1 have been found to reside in non-interacting ellipticals ([D’Ammando et al. 2017, 2018](#)). This result may support the low-inclination scenario for NLS1s, and might contradict the relation between merging/interaction and jet formation, or it could be that visible signatures of past interaction have relaxed. It is clear that more examples are needed to shed light on the host-AGN connection.

We selected SBS 0846 + 513 (RA = $8^{\text{h}}49^{\text{m}}58^{\text{s}}.1$, Dec = $+51^{\circ}08'25''.7$), a γ -ray emitting Narrow-Line Seyfert 1¹ at $z = 0.585$, with the goals of observing the host galaxy’s morphology and determining its black hole mass in a geometrically-independent way. It was unresolved in existing imagery and did not show clear evidence of interaction, and the new observations would put it near the high-redshift end of γ -NLS1 imaged at high resolution. Its relatively high redshift makes any investigation with ground-based telescopes difficult, but adaptive optics is a great help. An important requirement for adaptive optics is the presence of a nearby bright reference star that can be used to model the wave front and correct the images for atmospheric distortion. However, most jetted NLS1s are located well outside the Galactic plane, and they do not have any suitable reference star in the vicinities. For this reason, we decide to observe SBS 0846 + 513 with the Advanced Rayleigh Guided Ground Layer Adaptive Optics System (ARGOS) on the LBT Utility Camera in the Infrared (LUCII) camera mounted on the Large Binocular Telescope (LBT). This innovative system can produce a laser guide star that was used as reference for our observations.

The paper is organized as follows: The source is described in §2. In §3, we present the imaging and spectroscopic observations. The analysis is described in §4, including the galaxy modeling, isophote measurements, and black hole mass calculations. The discussion and interpretation are done in §5.

2 SBS 0846+513

SBS 0846 + 513 was already identified as a potential blazar by [Arp et al. \(1979\)](#), although it was considered as a BL Lac at high redshift, and its correct distance was estimated only with the Sloan Digital Sky Survey (SDSS) ([Schneider et al. 2003](#)). The source was already known for its extreme flaring activity, with a brightening of about 4 magnitudes in approximately a month ([Arp et al. 1979](#)), which was initially attributed to gravitational lensing effects ([Nottale 1986](#)). The source was identified as an NLS1 by [Zhou et al. \(2006\)](#) and [Yuan et al. \(2008\)](#), given its $H\beta$ FWHM of $\sim 1800 \text{ km/s}$, within the NLS1 definition. After the launch of *Fermi*, it was detected at γ -rays during its first observed flare ([Donato & Perkins 2011](#); [Foschini 2011](#)). The black hole mass of SBS 0846 + 513 was estimated both using the FWHM and the second-order moment of $H\beta$, and in both cases the estimate is approximately at $\sim 3 \times 10^7 M_{\odot}$, well within the typical range of NLS1s ([Yuan et al. 2008](#); [Foschini et al. 2015](#)). At radio frequencies the source has been monitored for years, showing high amplitude variability both in flux and in polarization ([Maune et al. 2014](#); [Angelakis et al. 2015](#); [Paliya et al. 2016](#)). At kiloparsec scale, it presents a compact structure with no diffuse emission ([Berton et](#)

¹ SBS 0846 + 513 has total absolute magnitude $M < -23$, so it is properly considered a quasar, but as we discussed above, we group Seyferts and quasars together in our discussions of NLS1.

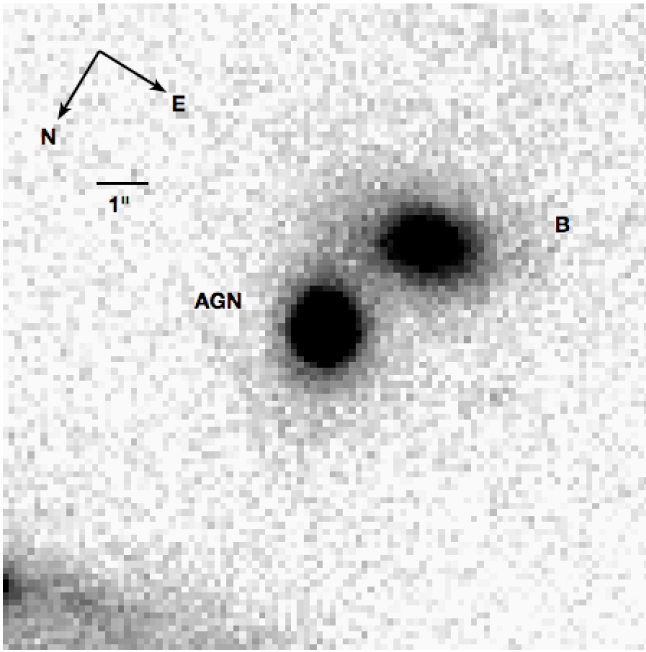


Figure 1. *J*-band view of the field surrounding SBS 0846 + 513. SBS 0846 + 513 is marked ‘AGN,’ and the projected companion ‘B.’ At bottom, an arm from a large, foreground spiral can be seen. The scale bar spans 1 arcsec.

al. 2018), while on parsec scale it shows a core-jet structure with superluminal motion and apparent velocity up to $\sim 8c$ (e.g., Lister et al. 2016). Regarding its host galaxy, no significant structure was detected with the *Hubble Space Telescope* (*HST*) (Maoz et al. 1993) in an observation made before the telescope’s spherical aberration was corrected. Our new data are the first high-resolution observations of this source.

3 OBSERVATIONS

3.1 Imaging

We observed SBS 0846 + 513 with the LUCI1 camera for two nights on 2016 December 14–15, as part of the commissioning run for ARGOS. LUCI1 and LUCI2 are twin instruments designed for both spectroscopy and imaging. In the imaging mode, they provide a 4×4 arcmin field of view.

On December 14, we observed with the infrared *Ks* and *J* filters, but the seeing was bad and the images unusable. On December 15, we observed with the *J* filter only. On this night, the seeing and image quality were good, and we obtained a total exposure time of 31.7 minutes for the science observations, with individual exposures of 10 s each. The image scale is 0.118 arcsec per pixel. Building up a composite Point Spread Function (PSF) from stars in the field, we obtain a PSF Full Width at Half-Maximum (FWHM) of 0.308 arcsec. The image reduction and PSF construction are described in §4.1

The target region is shown in Fig. 1. The NLS1, SBS 0846 + 513, is marked ‘AGN.’ Partially overlapping the AGN is a second galaxy, labelled ‘B’ in the image, that has a projected distance of 2.45 arcsec centre-to-centre.

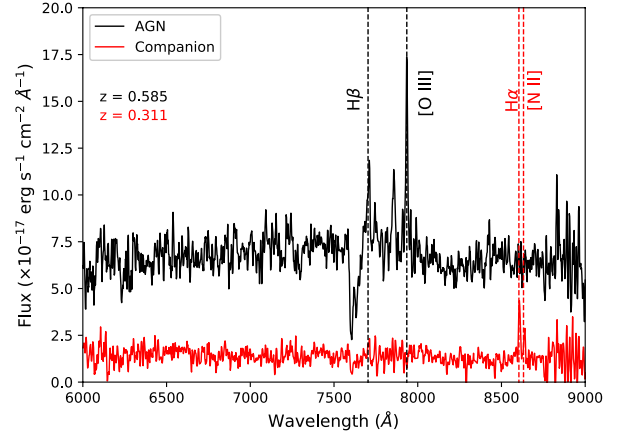


Figure 2. NOT spectra of the AGN (upper line, black) and the apparent companion (lower line, red). Identified emission lines are marked with dashed, vertical lines: $H\beta$ and $[O\text{ III}]$ in the AGN, $H\alpha$ and $[N\text{ II}]$ in the apparent companion. We measure a redshift of $z = 0.585$ for the AGN and $z = 0.311$ for Galaxy B.

3.2 Spectroscopy and Redshift

Because Galaxy B is projected to partially overlap the AGN, it raises the question of whether or not B is a physical companion, and possibly interacting. We addressed this spectroscopically, observing SBS 0846 + 513 with the Alhambra Faint Object Spectrograph and Camera (ALFOSC) on the Nordic Optical Telescope (NOT) on May 9, 2018. The spectrum was obtained with a 1 arcsec slit oriented at position angle 160° , to fit both SBS 0846 + 513 and Galaxy B in the slit at the same time. The spectrum interval covered was between 5650 and 10150 Å, with a resolution $R \sim 770$ and a total exposure time of 1800 s. After the standard bias and flat-field correction, the wavelength calibration was performed using a ThAr lamp. We flux calibrated the spectrum using as reference the standard star HD 93521.

The spectrum of the two sources is shown in Fig. 2. We clearly identify the AGN lines at $z = 0.585$, as expected. Both $H\beta$ and $[O\text{ III}]\lambda\lambda 4959, 5007$ are clearly visible, next to the telluric absorption by the atmosphere. In the putative companion, instead, neither line is visible at the same wavelength. Instead, we detected at 8604 and 8631 Å, two narrow emission lines compatible with redshifted $H\alpha$ and $[N\text{ II}]\lambda 6584$ at $z = 0.311$. In principle, the $H\beta$ region and the $[O\text{ III}]\lambda 5007$ Å line would also be visible in Galaxy B, but they are not detected in the spectrum, possibly suggesting the presence of internal absorption. Regardless of the reason these are not detected, Galaxy B is definitely not at the same redshift as SBS 0846 + 513.

4 ANALYSIS

4.1 Image Processing

The data reduction process for producing the science image follows the steps described by Georgiev et al. (2019) in their ARGOS commissioning paper. After a basic reduction, correcting for non-linearity and persistence effects, bad pixel masking and flat fielding, sky frames were created from exposures spaced about 10 minutes apart in order to negate effects by the rapidly-varying Near-Infrared (NIR) atmosphere. The best 164 exposures were used in this case.

Table 1. Statistics of sky and residuals. Columns– (1) Region or model residual. South, East, and West refer to source-free regions near the AGN. 1C and 2C residuals have the total model subtracted from the image and use the fitting region centred on the AGN. (2) Mean value. (3) Minimum value. (4) Maximum value. (5) Standard deviation. (6) Distance of region from the AGN. Note *a*–Modeled sky level for the 1C model is 1.24 ADU. Note *b*–Modeled sky level for the 2C model is 1.73 ADU.

(1) Region	(2) Mean (ADU)	(3) Minimum (ADU)	(4) Maximum (ADU)	(5) σ (ADU)	(6) Distance (arcsec)
East	1.47	-18.41	21.81	4.52	15
West	2.24	-20.32	16.1	4.41	16
South	3.03	-17.02	17.25	4.35	22
1C residual	0.00 ^a	-83.49	101.12	5.79	0
2C residual	0.00 ^b	-65.23	97.17	5.58	0

Bright sources, such as stars and galaxies (with pixel values $\sim 4\sigma$ above the background) were masked prior to combination. Several sky frames were used to subtract the sky in a group of exposures spaced within about 15 minutes.

Due in part to the extended spiral galaxy nearby and its effect on the flatfielding, the sky in source-free areas varies somewhat in the region around the AGN. At 15 arcsec east of the AGN, it has a mean of 1.47 Analog-to-Digital Units (ADU), 16 arcsec west of the AGN, the mean is 2.24 ADU, and 22 arcsec south of the AGN, the mean is 3.03 ADU. The large galaxy is to the north of the AGN, so no measurement is made there. The statistics for these regions is listed in Table 1. To minimize these effects in the analysis, we restrict the model fit (§4.3) to a region close to the AGN.

4.2 Photometric Calibration

We calibrated the *J*-band magnitude system using the 2-Micron All Sky Survey (2MASS) Extended Source Catalog and Point Source Catalog. Instrumental magnitudes for sources from our image were extracted with Source Extractor and compared to the 2MASS catalogs. Excluding the AGN (which is variable), Galaxy B (which is merged with the AGN in 2MASS), and one bright star that is saturated, nine sources in this field are found in the Point Source Catalog (PSC). Two of these are spiral galaxies and are also listed in the Extended Source Catalog (XSC). We adopt the XSC *J* magnitudes for these two and the PSC *J* magnitudes for the remaining seven. With these sources, we obtain a magnitude calibration with a standard deviation of $\sigma = 0.26$ mag.

4.3 Host + Nucleus Modeling

Because this active galaxy has a bright nucleus, any study of its morphology requires a fit to both the nucleus–modeled with the point spread function (PSF)–and the host galaxy. We use GALFIT (Peng et al. 2011) to perform a 2-dimensional fit to the image, simultaneously modeling the nucleus, the host galaxy, and Galaxy B, with the sky fitted as a constant value. Because of the spatial variations in the sky described in §4.1, we perform the fit over a region spanning 101×101 pixels (11.9×11.9 arcsec), centred on the AGN. This is wide enough to cover the visible extent of the AGN host and Galaxy B but narrow enough so that the sky variation within the region is small. The large, foreground spiral seen in the north corner of Fig. 1 and the region of brighter sky to the south of Galaxy B (which may include a low-surface-brightness source) are both masked out of the

fit, as are smaller, dimmer clumps. The PSF model is constructed as a composite of 16 isolated stars from across the field of view and has a Full Width at Half Maximum of 2.6 arcsec. It spans 19×19 pixels (2.2×2.2 arcsec) and is put into GALFIT with normal sampling.

To determine the morphology, two models of the host galaxy are tried. Model 1C is a one-component fit to the AGN host using a Sérsic model, while model 2C performs a two-component fit to the host, using a Sérsic bulge and an exponential disc. The Sérsic index, n , is a free parameter in both cases. Since we are not interested in the details of its morphology, Galaxy B is modeled with only single Sérsic component (with the index as a free parameter) in both cases, which leaves acceptably low residuals. Including separate bulge and disc components results in unreasonable fits. The sky is modeled as a constant value; allowing it to ‘tilt’ across the field does not improve the fit. The host galaxy is shown in the PSF-subtracted residual image in Fig. 3, along with the total residuals, formed by subtracting the complete model from the image. The fitting results are summarized in Table 2 for the AGN and Table 3 for Galaxy B, and the statistics of the residuals are listed in Table 1.

Absolute magnitudes and physical scales for both galaxies are presented in Table 4, using a cosmology of $H_0 = 71$, $\Omega_M = 0.27$, and $\Omega_{\text{vac}} = 0.73$. At the AGN’s redshift, the scale is 6.59 kpc/arcsec, while for Galaxy B, it is 4.53 kpc/arcsec. To calculate the absolute magnitudes, we adopt *K*-corrections for the AGN nucleus from Glikman, Helfand, & White (2006) and for the AGN host and Galaxy B from Mannucci et al. (2001). For the purposes of the *K*-correction, we assume the AGN host is an E-type galaxy for the 1C model and an Sa-type galaxy for the 2C model, while Galaxy B is treated as an Sa type.

In addition to the two-dimensional modeling, we examine the AGN’s radial profile and isophote structure. Fig. 4 and Fig. 5 show the radial surface brightness (μ) profiles of the AGN for the 1C and 2C models, respectively, measured using IRAF’s ellipse task with circular annuli. Plots are included of the image (with the sky and the Galaxy B model subtracted), the total model, and the separate components of that model–the host model (1C: Sérsic only; 2C: Sérsic bulge and exponential disc) and the nuclear model (stellar PSF). The profile is taken out to an angular distance of 3 arcsec from the centre of the nucleus, corresponding to a projected distance of 20 kpc at the redshift of the source. The bottom portion of the figure shows the difference between the image and the total model for each isophote: $\Delta\mu = \mu_{\text{image}} - \mu_{\text{total model}}$.

In Fig. 6, IRAF’s ellipse task is also used to measure the Fourier a_4/a parameter of the isophotes of the PSF-subtracted host. Negative values of a_4/a indicate boxiness in a given isophote, a more rectangular deviation from an ellipse, while positive values indicate discy, lemon-shaped isophotes. An overall discy trend to the isophotes is associated with the presence of galactic discs. The convolution of the bright centre of the galaxy with the PSF biases the shape of the innermost isophotes, so we do not plot isophotes closer than 0.4 arcsec (2.6 kpc) from the centre. The vertical axis is scaled by a factor of 100×, and the dashed horizontal line at $a_4/a = 0$ separates the positive (discy) values from negative (boxy) values.

4.4 Black Hole Mass

We use three methods to determine the central black hole mass–the correlation with the host bulge, and two correlations with the Sérsic index. Detailed results are shown in Table 5. The relationship between host spheroidal luminosity and black hole mass is given by

Table 2. Summary of AGN model fits. Columns–(1) Model type: 1C uses a one-component Sérsic fit to the AGN host, listed under ‘Bulge,’ because of its high Sérsic index. Model 2C uses two AGN host components—a Sérsic bulge and an exponential disc. (2) Reduced χ^2 of the fit. (3) Nuclear J magnitude. (4)–(11) J magnitude (m), radius (r), Sérsic index (n), and ellipticity (ϵ) for host bulge and disc. $1-\sigma$ uncertainties are listed in brackets. Parameters that are held fixed are listed in parentheses. Subscripts p , b , and d refer to nucleus (PSF), bulge, and disc, respectively.

(1)	(2)	(3)	(4)	(5)	(6)	(7)	(8)	(9)	(10)	(11)
Model	χ^2/ν	Nucleus (PSF) m_p (mag)	m_b (mag)	Bulge r_b (")	n_b	ϵ_b	m_d (mag)	disc r_d (")	n_d	ϵ_d
1C	1.2	20.3 [< 0.1]	20.3 [< 0.1]	1.1 [0.1]	3.4	0.41	–	–	–	–
2C	1.1	20.4 [< 0.1]	21.3 [< 0.1]	0.1 [< 0.1]	7.3	0.86	20.9 [< 0.1]	0.6 [< 0.1]	(1)	0.30

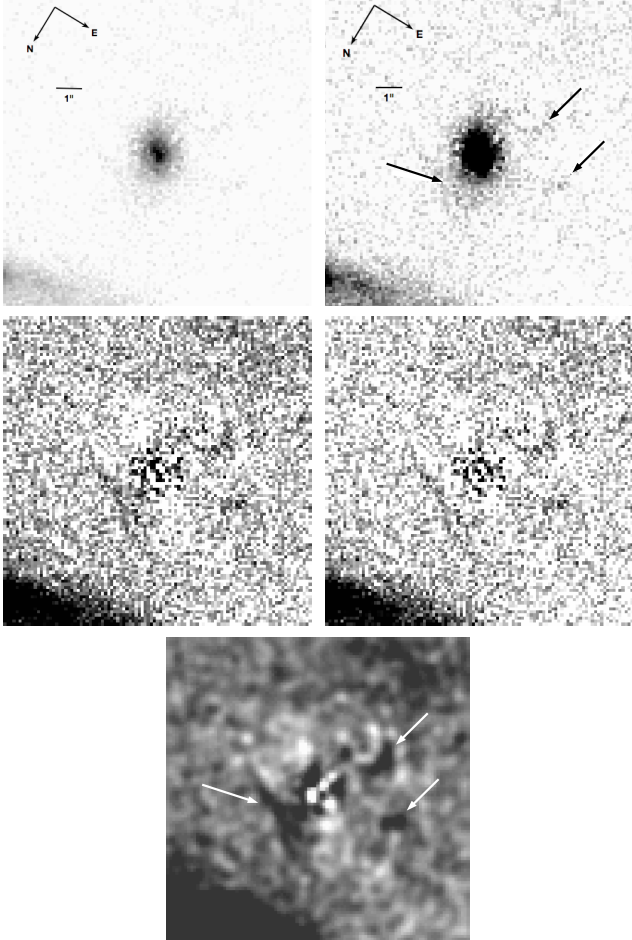


Figure 3. View of the AGN host galaxy and residuals. The field of view is the same as in Fig. 1. *Top row:* The PSF and Galaxy B models have been subtracted, showing the AGN host galaxy. *Top left:* Low-contrast image, showing the inner features of the host. The noise 1 arcsec from the host centre is due to scaling up the faint edges of the stellar PSF model. *Top right:* High-contrast image, emphasizing the outer envelope. Three clumps of material are indicated by the arrows. The lower two are just visible in Fig. 1 but are clearer here. The clump to the southeast of the AGN is hidden by Galaxy B in the original image. *Middle row:* Residuals made by subtracting the total model. An inverted color scheme (blackier is brighter) is used, in keeping with the images at top. *Middle left:* 1C model residual. *Middle right:* 2C model residual. The higher noise at the centre, extending to a radius of 1 arcsec, is due to the PSF model. The apparent structures noted in the top row stand out above the variations in the sky and residual. *Bottom:* 1C model residual with 3-pixel Gaussian smoothing. The clumps of material noted before (marked with arrows) are more visible.

Table 3. Summary of model fits for Galaxy B. Columns–(1) Model type (same as above). (2) Apparent J magnitude. (3) Half-light radius. (4) Sérsic index. (5) Ellipticity. $1-\sigma$ uncertainties are listed in brackets.

(1)	(2)	(3)	(4)	(5)
Model	m_B (mag)	r_B (")	n_B	ϵ_B
1C	20.1 [< 0.1]	1.2 [< 0.1]	2.3	0.33
2C	20.1 [< 0.1]	1.1 [< 0.1]	2.2	0.34

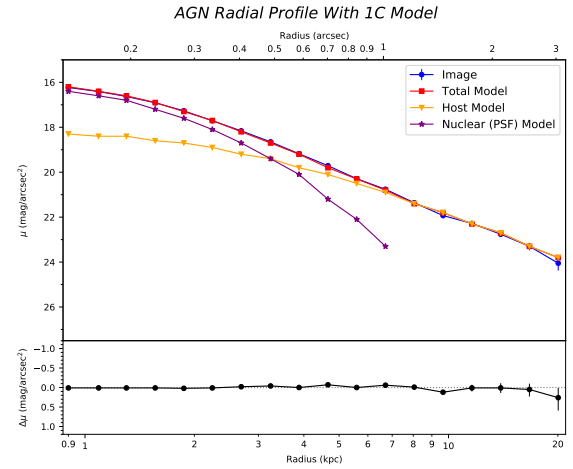


Figure 4. Radial surface brightness (μ) plot of the AGN image and components for the 1C (Sérsic) model, using circular annuli. The upper plot shows the profiles of the image (with the sky and the Galaxy B model removed), the total model, and the model’s individual components. The lower plot shows the difference in surface brightness between the image and the total model ($\Delta\mu = \mu_{\text{image}} - \mu_{\text{total model}}$). The horizontal axis is marked in both arcseconds (top scale) and projected kpc for the redshift of the AGN (bottom scale) for both plots. The vertical range is scaled to match Fig. 5 for ease of comparison. Error bars are given for the image and $\Delta\mu$. The single Sérsic model provides a good match to the profile out to about 3 arcsec (20 kpc). Beyond this, the image profile is lost in the sky variation.

Marconi & Hunt (2003) as

$$\log \frac{M_{\text{BH}}}{M_{\odot}} = a + bX, \quad (1)$$

where for the J -band, $a = 8.26 \pm 0.07$, $b = 1.14 \pm 0.12$, $X = \log L_{J,\text{bulge}} - 10.7$, M_{BH} represents the black hole mass, M_{\odot} is the Sun’s mass, and $L_{J,\text{bulge}}$ is the J -band spheroidal luminosity. In

Table 4. Derived quantities for the AGN and Galaxy B. Columns—(1) Model (same as above). (2) J -band absolute magnitude of the AGN nucleus. (3)–(6) J -band absolute magnitudes (M), and radii (r), for the AGN bulge and disc. (7)–(8) Bulge-to-Total ratio and total absolute magnitude for the AGN host. (9)–(10) J -band absolute magnitude and radius for galaxy B. $1-\sigma$ uncertainties are listed in brackets. Subscripts are the same as above.

(1)	(2)	(3)	(4)	(5)	(6)	(7)	(8)	(9)	(10)
Model	Nucleus M_n (mag)	Bulge M_b (mag)	r_b (kpc)	disc M_d (mag)	r_d (kpc)	B/T	M_{host} (mag)	Galaxy B M_B (mag)	r_B (kpc)
1C	-22.4	-22.7	7.5 [0.5]	–	–	1.00	-22.7	-21.1	5.2 [0.2]
2C	-22.3	-21.6	0.7 [0.1]	-22.0	4.0 [0.1]	0.41	-22.6	-21.1	5.1 [0.2]

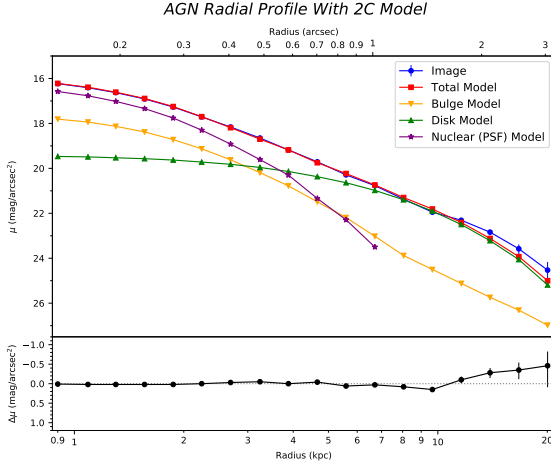


Figure 5. Radial surface brightness (μ) plot of the AGN image and components for the 2C (Sérsic bulge + exponential disc) model. The plot layout and scale are the same as in Fig. 4. The Sérsic + exponential disc model is a good match to the profile out to about 1.8 arcsec (12 kpc). From there to about 3 arcsec (20 kpc), there is excess light from the filament-like structure to the north and imperfectly-subtracted light in Galaxy B, both shown in the residual image in Fig. 3. Though the 2C model’s radial profile diverges from the image in the outer radii, it provides a better overall fit in two dimensions than the 1C model does.

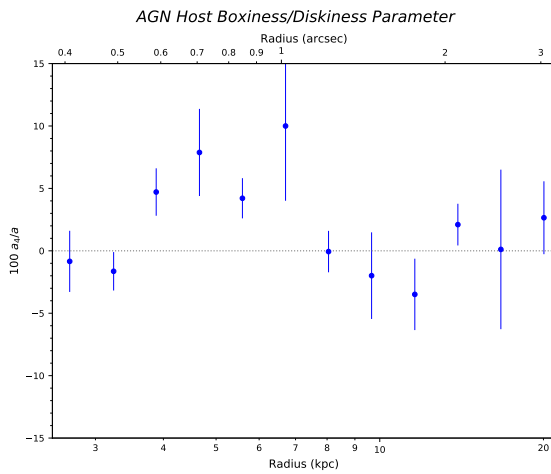


Figure 6. Isophote boxiness/diskiness parameter as a function of semi-major axis. Negative values of $a_4 < 0$ indicate boxiness, while positive values indicate diskiness. Using the criteria of Bender et al. (1989), we can assign a characteristic value of $a_4/a \sim 0.05 - 0.08$, which is discy.

Table 5. Central black hole mass of the AGN, calculated by different methods: ‘Bulge luminosity’ is the black hole mass/bulge luminosity relation; ‘Sérsic linear’ is the linear fit to the black hole mass/Sérsic index relation; ‘Sérsic quadratic’ is the quadratic fit to the latter. Models are the same as above. Mass uncertainties (listed in brackets) account for uncertainties in the proxy and statistical uncertainties in the input parameter, but they cannot account for systematic errors in the input parameter.

Method	Model	$\log(M_{\text{BH}}/M_{\odot})$
Bulge luminosity	1C	8.19 [0.08]
Bulge luminosity	2C	7.70 [0.10]
Sérsic linear	1C	7.96 [0.12]
Sérsic quadratic	1C	8.16 [0.13]

terms of spheroidal magnitude, $M_{J,\text{bulge}}$, this becomes

$$\log \frac{M_{\text{BH}}}{M_{\odot}} = 0.46(M_{J,\odot} - M_{J,\text{bulge}}) - 3.94, \quad (2)$$

Using $M_{J,\odot} = 3.67$ for the Sun’s magnitude, we obtain a black hole mass of $1.55 \times 10^8 M_{\odot}$ for the 1C model and $4.97 \times 10^7 M_{\odot}$ for the 2C model.

The radial profile method of Graham & Driver (2007) correlates the Sérsic index, n , with the black hole mass. They fit both linear (their Equ. 4) and quadratic (their Equ. 7) relationships to the data. The linear fit gives

$$\log \frac{M_{\text{BH}}}{M_{\odot}} = (2.68 \pm 0.40) \log \frac{n}{3} + (7.82 \pm 0.07), \quad (3)$$

while the quadratic fit is

$$\log \frac{M_{\text{BH}}}{M_{\odot}} = (7.98 \pm 0.09) + (3.70 \pm 0.46) \log \frac{n}{3} - (3.10 \pm 0.84) \left(\log \frac{n}{3} \right)^2. \quad (4)$$

As shown in Table 5, model 1C leads to a mass of $9.09 \times 10^7 M_{\odot}$ for the linear fit or $1.46 \times 10^8 M_{\odot}$ for the quadratic fit. Since the two-component model bulge is smaller than the PSF width, we do not calculate profile-derived masses for model 2C.

5 DISCUSSION

5.1 Host Galaxy

In interpreting the relationship of these gamma-ray emitters to the broader population of NLS1, it is important to compare their morphologies. But very few of the gamma-ray emitters’ hosts have been resolved, because the fraction of NLS1 known to emit gamma-rays peaks at $z \sim 0.5 - 0.7$, where their hosts become harder to distinguish, and high-resolution observations such as these are necessary.

Narrow-Line Seyfert 1s at low redshift have been found to reside primarily in spiral galaxies, similar to the overall population of Seyfert 1s. Crenshaw, Kraemer, & Gabel (2003) and Deo, Crenshaw, & Kraemer (2006) have only one clear E type in their NLS1 samples. Olguín-Iglesias et al. (2017) has one classified as SB0.

How does SBS 0846+513’s morphology compare to lower-redshift NLS1? As shown in Table 2, the one-component (1C) and two-component (2C) models of the AGN have similar goodness of fit, with a small improvement in the 2C model. The one-component model finds the AGN host galaxy to be roughly of the de Vaucouleurs profile, with an overall Sérsic index of 3.4. The two-component model uses an exponential disc and finds the bulge to have a steeper Sérsic index of 7.3, but the bulge is smaller than the PSF width, so we cannot do much interpretation of it. The bulge-to-total ratio of 0.41 (and to the extent we can interpret it, the bulge Sérsic index) is consistent with an Sab Hubble type (Weinzirl et al. 2009). Using the 6dF luminosity function of Jones et al. (2006) and a Hubble constant of $H_0 = 71$ km/s/Mpc, we obtain $M_J^* = -23.6$, while the host galaxy of SBS 0846 + 513 has a total magnitude of -22.7 (1C model) or -22.6 (2C)². This puts the host at 1 mag fainter than M_J^* .

The radial profile in Fig. 4 shows a good fit of the 1C model to the image out to 3 arcsec (20 kpc). Beyond this point, the variations in the background produce some regions of negative values in the sky-subtracted image, which we can’t display in magnitude form. The 2C model (Fig. 5) gives a close fit over most of the isophotes but shows some divergence at the outermost radii, where the model is too faint. Still, the 2C model has a slightly better reduced χ^2 than the 1C model in the two-dimensional fit.

We next examine the radial variation of the isophotes’ a_4/a parameter (Fig. 6), which is associated with boxy (negative) or discy (positive) isophotes. We disregard the central 0.3 arcsec, where the isophote shapes are likely to be dominated by convolution with the PSF. We see that a_4/a has a roughly-peaked distribution, rising from ~ 0 close to the centre, to large positive values in the $4 < r < 7$ kpc region, beyond which it declines irregularly. Though the graph is not smooth, under the criteria of Bender et al. (1989), we can assign a characteristic value of $a_4/a \sim 0.08$, and this strengthens the evidence for a disc.

In Fig. 3, we show residuals created by subtracting the PSF and Galaxy B models (top row) and the total model (middle and bottom rows) from the image. In the top row, we can see more clearly some clumps of material, marked by arrows. The lower two are just visible in Fig. 1 but are clearer in the residual, while the third (southeast of the AGN) is normally covered by Galaxy B until that model is subtracted. The extended features to the northwest and southeast of the AGN could be spiral arms. They’re on opposite sides, at about the same distance from the nucleus, but their shapes aren’t symmetrical and could show a disturbance. These three features are only of low significance ($\leq 1\sigma$ above sky level), and it would be interesting to see them in a deeper image.

Another interpretation of the hook-shaped pattern southeast of the AGN could be as a feature of Galaxy B. The outer isophotes of this galaxy have a slightly asymmetrical appearance to the eye, extending a bit farther to the west than the east. Our attempts to account for this in GALFIT (such as adding Fourier components or a non-concentric bulge and disc) either failed to improve the fit or kept it from converging.

The residual statistics for the unmasked regions are listed in the

bottom two rows of Table 1. There is no systematic offset from the sky level, though there is a higher standard deviation compared to the neighboring source-free regions. Some of this comes from noise in the PSF model for the nucleus, which is scaled in brightness during the fit. The noisy disc at the centre of the fitting region in Fig. 3 (middle row) results from the scaled-up PSF noise and extends out to a radius of 1 arcsec. The 2C model leaves a residual with a slightly lower standard deviation than the 1C model does, but then its PSF (which is a source of noise) is fainter by 0.1 mag. The brighter region to the south of Galaxy B, an area masked from the model fit, includes some low-surface-brightness sources that are just outside the cropped field.

So in its morphology, SBS 0846 + 513 does not appear obviously different from the common spiral galaxies of low-redshift NLS1. The bulge + disc model fits it slightly better than the spheroidal model, the isophotes show a discy structure in their Fourier components, and there are possible indications of spiral structure. Thus we tentatively conclude that the host of SBS 0846 + 513 is a bulge + disc galaxy. Either deeper ground-based observations with full adaptive optics or space-based observations with the *Hubble Space Telescope* or the *James Webb Space Telescope* would improve the resolution and the model of the galactic bulge, which is unresolved here.

5.2 AGN Environment

We considered whether or not SBS 0846 + 513 has a companion, perhaps involved in a merger that could have triggered its active phase. In Fig. 1, we see that Galaxy B is separated from SBS 0846 + 513 by a projected distance of 2.45 arcsec. Their proximity has caused problems in the past. In fact, SBS 0846 + 513 was once (Hewitt & Burbidge 1989) placed at a redshift of $z = 1.86$, due to the contamination of its spectrum by Galaxy B, whose redshift was roughly modeled as 0.235 in prior papers. At the resolution of the LBT, there is still a very slight overlap, and the possibility of a merger is interesting, given the role mergers sometimes play in triggering AGN.

From our spectroscopy (§3.2), we find the redshift of SBS 0846 + 513 is $z = 0.585$, using H β and [OIII] lines, but the redshift of Galaxy B is 0.311, using H α and [NII] lines. So the two galaxies are only visual companions, which are not interacting with each other.

Some of the three features marked in Fig. 3 could be dwarf companions of the AGN. If so, it would be consistent with the studies that show a majority of γ -NLS1 have signs of mergers or interactions (Komossa 2018). The small clump to the east lies at a projected distance of 23 kpc (3.5 arcsec) from the AGN. We have leaned towards interpreting the longer features to the northwest and southeast as arms of the AGN host, but it is possible they are also companions, if they are at the AGN redshift at all. A 3-pixel Gaussian smoothing is applied to the image in the bottom row to show them better.

5.3 Black Hole Mass

Earlier mass estimates for SBS 0846 + 513 have come from a variety of methods. Zhou et al. (2005) puts its mass at $8.2 \times 10^6 M_\odot$ using the Broad-Line Region (BLR) H β linewidth, $5.2 \times 10^7 M_\odot$ using the $M_{\text{BH}}-\sigma_*$ relation with the Narrow-Line Region [OIII] to get stellar motion in the bulge, or $4.3 \times 10^7 M_\odot$ using the $M_{\text{BH}}-M_{\text{bulge}}$ relation with the elliptical galaxy mass-to-light ratio and a host template spectrum. Yuan et al. (2008) obtain $2.5 \times 10^7 M_\odot$ using the BLR H β linewidth, which is close to the $3.2 \times 10^7 M_\odot$ calculated by Foschini et al. (2015). Using the estimates of black hole mass uncertainties by

² The small discrepancy comes from the different K -corrections for the morphologies.

Vestergaard (2004), both of these are consistent with the non-BLR masses of Zhou et al. (2005). Shen et al. (2011) derive mass estimates for SBS 0846 + 513 based on *Sloan Digital Sky Survey* spectra, including H β and MGI-derived masses by a variety of calibrations. These range from 5.6×10^7 – $9.7 \times 10^7 M_{\odot}$. These are slightly higher than the masses discussed above, but given their uncertainties, the low end of this range is consistent with the H β estimate of Zhou et al. (2005).

As mentioned in §1, it has been argued that the narrow widths of NLS1s' permitted lines might not be due to smaller black hole masses but to geometry—that these galaxies are viewed nearly pole-on to a disc-like BLR, minimizing the Doppler effects and leading to an underestimate of the black hole mass. In gamma-ray emitting NLS1s, at least, we are more likely to have a nearly pole-on view of the black hole, since we must be looking along the radio jet. But since we are able to resolve much of the host galaxy in the case of SBS 0846 + 513, we can derive measures of the black hole mass that are independent of the BLR flattening and orientation, using the correlations with bulge luminosity and radial profile.

Being derived from the host galaxy, the masses we calculate in Table 5 are independent of BLR geometry and viewing angle. Using our preferred (bulge + disc) host morphology, the mass-luminosity relation of the bulge gives us the lowest of the four mass estimates. At $5.0 \times 10^7 M_{\odot}$, it is comparable to the upper end of the range of masses from the prior work on this AGN. The mass-luminosity relation assumes a classical bulge, and pseudobulges tend to have smaller black hole masses for their luminosity (Mathur et al. 2012). Since our bulge is effectively unresolved (the effective radius is narrower than the PSF), we don't know if it is classical or pseudo, and so the black hole mass could be lower. On the other hand, if we accept the one-component model, then we count the luminosity of the entire host galaxy as the 'bulge,' and we obtain our highest estimate, $1.6 \times 10^8 M_{\odot}$. The Sérsic index methods applied to the one-component model give results that are close to this upper value, but because the bulge in the two-component model is so narrow, we don't try to derive a mass from its profile. So the biggest variation in the mass estimates comes from adopting either the one or the two-component model. In the end, the low end of our mass estimates (our preferred model) is consistent with previous results, while the high end is a factor of two or three times larger than these. This indicates that the H β -derived masses for this source are *not* substantially underestimated.

How does the mass of SBS 0846 + 513 compare with other NLS1 in general and gamma-ray emitters in particular? Based on a sample selected by Rakshit et al. (2017), Berton et al. (2020) report on their study of 3933 NLS1 whose H β lines fit a Gaussian or Lorentzian profile, using SDSS data extending out to a redshift of $z = 0.8$. Of these, none has a black hole mass greater than $10^8 M_{\odot}$. Even our lowest mass estimate for SBS 0846 + 513 would make it more massive than all but 1.8 per cent (72 out of 3932) of the complete Berton et al. (2020) sample. A better comparison would account for the variation in mass distribution with redshift. Restricting ourselves to sources within a redshift range of ± 0.1 from SBS 0846 + 513 ($0.485 < z < 0.685$), we see that it is, at minimum, more massive than all but 4.5 per cent (35 out of 776) of NLS1 in that range. Regarding gamma-ray emitting NLS1, the 10 other γ -NLS1 with measured masses (Foschini et al. 2015) range from $1.4 \times 10^7 M_{\odot}$ up to $1.15 \times 10^8 M_{\odot}$. Our mass calculations for SBS 0846 + 513 puts it at least in the upper half of this group (more massive than 5 out of 10, at the low end), and at the high end, more massive than all of the others.

Komossa (2018) compiles mass estimates for two γ -NLS1 (1H 0323 + 342 and PKS 1502 + 036) whose black holes have been

measured with several techniques, including host galaxy correlations (original host analyses by León Tavares et al. 2014 and D'Ammando et al. 2018, respectively), single-epoch H β spectroscopy, SED modeling, and others. It is interesting to note that the host-galaxy-derived methods return much higher masses than the single-epoch H β spectra in those cases: by one order of magnitude for 1H 0323 + 342 and by two orders of magnitude for PKS 1502 + 036. In fact, the host galaxy correlations lead to the highest mass estimates of *any* of the methods on the list. Since single-epoch spectra are orientation-dependent while the host galaxy methods are not, one possibility is that the spectra are underestimating the black hole mass. However, the H β results in these two cases are more consistent with mass results from several other methods, as we expect. The consistency is good for 1H 0323 + 342; in the case of PKS 1502 + 036, the H β result returns the lowest mass of four methods across seven studies, but the greatest difference is between H β and the host galaxy result.

On the other hand, the host galaxy methods could be overestimating the black hole mass. León Tavares et al. (2014) find similar goodness-of-fit for the elliptical (bulge) and spiral (bulge + disc) models for 1H 0323 + 342's host, and they choose the elliptical model for simplicity. The bulge in the *J*-band spiral model is 1.5 mag fainter than in the elliptical model, and it has a Sérsic index of $n = 0.88$, which is consistent with a pseudobulge. For PKS 1502 + 036, D'Ammando et al. (2018) find a lower χ^2/ν for their spiral model than the elliptical model. Choosing the spiral would make the bulge 0.4 mag fainter. The Sérsic index is fixed at $n \equiv 4$ in this case, so we cannot tell from their report if the bulge would be classical or a pseudobulge. However, Olguín-Iglesias, Kotilainen, & Chavushyan (2020) find a spiral host with a bulge whose Sérsic index is close to 1, indicating a pseudobulge and decreasing the black hole mass. In both of these cases, then, using the spiral model to derive the black hole mass would be justifiable, and it would return a lower result.

It would be interesting to make more general comparisons between the masses of the known γ -NLS1 and the non- γ -emitters, but we must be cautious using even the H β -derived masses for each group, because of different assumed values for the virial factor, f . For example, the Berton et al. (2020) sample of NLS1 uses $f = 3/4$, while the γ -NLS1 masses of Foschini et al. (2015) are calculated using $f = 3.85$. Since f is related, in part, to the inclination angle of the Broad-Line Region, and the γ -NLS1 must be viewed close to pole-on, then these different values may be appropriate. But more work is needed, and it would be good to have a larger set of orientation-independent measures of black hole mass as a comparison.

It should be noted that there is a very strong statistical argument that the majority of Narrow-Line Seyfert 1s cannot have BH masses as high as Broad-Line Seyfert 1s (BLS1) and simply be underestimated due to their geometry. As pointed out by Komossa et al. (2006), if NLS1s were just the face-on analogues of BLS1s and narrower Balmer line widths because the Broad Line Region was flattened and viewed close to pole-on, then we should see a large fraction of beamed NLS1s. In fact, more NLS1s would be seen as beamed than BLS1s, because they would be the population with more face-on sources. Yet the opposite is the case. Studies consistently find that the fraction of radio-loud sources is smaller in NLS1s.

So SBS 0846 + 513 has a massive black hole, larger than most NLS1, but consistent with estimates of the other gamma-ray emitting NLS1. The H β -derived masses for this source are not greatly underestimated.

5.4 Variability

SBS 0846+513 shows strong variability at all wavelengths, from radio (e.g., Angelakis et al. 2015) to mid-IR (see Caccianiga et al. 2015) to γ -rays (see Foschini et al. 2015). Comparing the photometry of SBS 0846+513 between our observations and the 2MASS Extended Source Catalog, we see the AGN nucleus has dimmed significantly since the 2MASS observation of 1998 December 23. The 2MASS observations are not able to resolve the AGN and Galaxy B, so we subtract the light we measure for the host galaxies of these two and find the nucleus in 1998 had $J = 15.9$. So it has dimmed by 4.4 mag to the $J = 20.3$ we observed on 2016 December 15. SBS 0846+513 is known to have exceptional changes in the optical (e.g., the 4-magnitude variation in about a month recorded by Arp et al. 1979), so this level of variability is not unusual for this object and is well within the historical range.

6 CONCLUSIONS

We observed the Narrow-Line Seyfert 1 galaxy SBS 0846+513 in the J -band with the LUCI1 camera, aided by laser-guide ground-layer adaptive optics system, ARGOS, on the Large Binocular Telescope. The galaxy has a significant gamma-ray emission, likely from a relativistic jet. Very little is known about the host galaxies of the γ -NLS1 and how they fit into the broader population of normal NLS1.

The host galaxy is resolved. There is a slight preference for the spiral model over the elliptical, and we see evidence for what may be spiral arms. This and its discy isophotes argue for a bulge + disc host galaxy, which is consistent with most NLS1 at lower redshift, even though relativistic jets are more common in ellipticals. Space-based observations from the *Hubble Space Telescope* or the *James Webb Space Telescope* would be useful to improve the resolution of the host, model the bulge, and look for signs of galaxy interactions.

Using correlations between black hole mass on the one hand and bulge luminosity and Sérsic index on the other, we find it harbors a central black hole with a mass likely around $5.0 \times 10^7 M_{\odot}$, but possibly as high as $1.6 \times 10^8 M_{\odot}$. These measurements are independent of the viewing angle to the Broad Line Region and therefore avoid any biases due to BLR geometry, and they indicate that the $H\beta$ -derived masses for this object are not greatly underestimated. The mass lies at the high end of the normal NLS1 range but is consistent with other γ -NLS1 masses.

ACKNOWLEDGEMENTS

T. S. H. would like to thank Luigi Foschini for many useful discussions, especially on the interpretation of the mass.

S. A. acknowledges financial support from the Centre for Research & Development in Mathematics and Applications (CIDMA) strategic project UID/MAT/04106/2019 and from Enabling Green E-science for the Square Kilometre Array Research Infrastructure (EN-GAGESKA), POCI-01-0145-FEDER-022217, funded by the Programa Operacional Competitividade e Internacionalização (COMPETE 2020) and FCT, Portugal.

This paper is based on observations made with the Large Binocular Telescope and the Nordic Optical Telescope. The Large Binocular Telescope is managed by the Large Binocular Telescope Observatory Collaboration, headquartered at the University of Arizona, in Tucson, Arizona, U.S.A. The Nordic Optical Telescope is operated by the Nordic Optical Telescope Scientific Association at the Observatorio del Roque de los Muchachos, La Palma, Spain, of the

Instituto de Astrofísica de Canarias. Our research has made use of the NASA/IPAC Extragalactic Database (NED), which is funded by the National Aeronautics and Space Administration and operated by the California Institute of Technology.

DATA AVAILABILITY

The data underlying this article will be shared on reasonable request to the corresponding author.

REFERENCES

- Angelakis E., Fuhrmann L., Marchili N., Foschini L., Myserlis I., Karanavitis V., Komossa S., et al., 2015, *A&A*, 575, A55
- Arp H., Sargent W. L. W., Willis A. G., Oosterbaan C. E., 1979, *ApJ*, 230, 68
- Abdo A. A., Ackermann M., Ajello M., Axelsson M., Baldini L., Ballet J., Barbiellini G., et al., 2009, *ApJ*, 699, 976
- Antón S., Browne I. W. A., Marchã M. J., 2008, *A&A*, 490, 583
- Berton M., Congiu E., Järvelä E., Antonucci R., Kharb P., Lister M. L., Tarchi A., et al., 2018, *A&A*, 614, A87
- Berton M., Congiu E., Ciroi S., Komossa S., Frezzato M., Di Mille F., Antón S., et al., 2019, *AJ*, 157, 48
- Berton M., Björklund I., Lähteenmäki A., Congiu E., Järvelä E., Terreran G., La Mura G., 2020, *CoSka*, 50, 270
- Bender R., Surma P., Doebereiner S., Moellenhoff C., Madejsky R., 1989, *A&A*, 217, 35
- Boller T., Brandt W. N., Fabian A. C., Fink H. H., 1997, *MNRAS*, 289, 393
- Boroson T. A., Green R. F., 1992, *ApJS*, 80, 109
- Brandt W. N., Boller T., Fabian A. C., Ruszkowski M., 1999, *MNRAS*, 303, L53
- Caccianiga A., Antón S., Ballo L., Foschini L., Maccacaro T., Della Ceca R., Severgnini P., et al., 2015, *MNRAS*, 451, 1795
- Calderone G., Ghisellini G., Colpi M., Dotti M., 2013, *MNRAS*, 431, 210
- Chiaberge M., Gilli R., Lotz J. M., Norman C., 2015, *ApJ*, 806, 147
- Crenshaw D. M., Kraemer S. B., Gabel J. R., 2003, *AJ*, 126, 1690
- D’Ammando F., Acosta-Pulido J. A., Capetti A., Raiteri C. M., Baldi R. D., Orienti M., Ramos Almeida C., 2017, *MNRAS*, 469, L11
- D’Ammando F., Acosta-Pulido J. A., Capetti A., Baldi R. D., Orienti M., Raiteri C. M., Ramos Almeida C., 2018, *MNRAS*, 478, L66
- Decarli R., Dotti M., Fontana M., Haardt F., 2008, *MNRAS*, 386, L15
- Deo R. P., Crenshaw D. M., Kraemer S. B., 2006, *AJ*, 132, 321
- Donato D., Perkins J. S., 2011, *ATel*, 3452
- Ferrarese L., Merritt D., 2000, *ApJL*, 539, L9
- Foschini L., 2011, *nlsg.conf*, 24
- Foschini L., Berton M., Caccianiga A., Ciroi S., Cracco V., Peterson B. M., Angelakis E., et al., 2015, *A&A*, 575, A13
- Gallo L., 2018, *rnl.conf*, 34
- Georgiev I. Y., Neumayer N., Gässler W., Rabien S., Busoni L., Bonaglia M., Ziegler J., et al., 2019, *MNRAS*, 484, 3356
- Glikman E., Helfand D. J., White R. L., 2006, *ApJ*, 640, 579
- Goodrich R. W., 1989, *ApJ*, 342, 224
- Graham A. W., Driver S. P., 2007, *ApJ*, 655, 77
- Grupe D., Mathur S., 2004, *ApJL*, 606, L41
- Hewitt A., Burbidge G., 1989, *ApJS*, 69, 1
- Järvelä E., Lähteenmäki A., Berton M., 2018, *A&A*, 619, A69
- Järvelä E., Berton M., Ciroi S., Congiu E., Lähteenmäki A., Di Mille F., 2020, *A&A*, 636, L12
- Jones D. H., Peterson B. A., Colless M., Saunders W., 2006, *MNRAS*, 369, 25
- Komossa S., Voges W., Xu D., Mathur S., Adorf H.-M., Lemson G., Duschl W. J., et al., 2006, *AJ*, 132, 531
- Komossa S., 2018, Revisiting narrow-line Seyfert 1 galaxies and their place in the Universe (NLS1-2018), 15
- Kormendy J., Ho L. C., 2013, *ARA&A*, 51, 511

- Kotilainen J. K., León-Tavares J., Olgún-Iglesias A., Baes M., Anórve C., Chavushyan V., Carrasco L., 2016, *ApJ*, 832, 157
- Krongold Y., Dultzin-Hacyan D., Marziani P., 2001, *AJ*, 121, 702
- Laor A., 2000, *ApJL*, 543, L111
- Lanz L., Ogle P. M., Alatalo K., Appleton P. N., 2016, *ApJ*, 826, 29
- León Tavares J., Kotilainen J., Chavushyan V., Añorve C., Puerari I., Cruz-González I., Patiño-Alvarez V., et al., 2014, *ApJ*, 795, 58
- Lister M. L., Aller M. F., Aller H. D., Homan D. C., Kellermann K. I., Kovalev Y. Y., Pushkarev A. B., et al., 2016, *AJ*, 152, 12
- Magorrian J., Tremaine S., Richstone D., Bender R., Bower G., Dressler A., Faber S. M., et al., 1998, *AJ*, 115, 2285
- Mannucci F., Basile F., Poggianti B. M., Cimatti A., Daddi E., Pozzetti L., Vanzi L., 2001, *MNRAS*, 326, 745
- Maoz D., Bahcall J. N., Doxsey R., Schneider D. P., Bahcall N. A., Lahav O., Yanny B., 1993, *ApJ*, 402, 69
- Marconi A., Hunt L. K., 2003, *ApJL*, 589, L21
- Mathur S., 2000, *MNRAS*, 314, L17
- Mathur S., Fields D., Peterson B. M., Grupe D., 2012, *ApJ*, 754, 146
- Maune J. D., Eggen J. R., Miller H. R., Marshall K., Readhead A. C. S., Hovatta T., King O., 2014, *ApJ*, 794, 93
- Morganti R., Oosterloo T. A., Oonk J. B. R., Frieswijk W., Tadhunter C. N., 2015, *ASPC*, 499, 125
- Nottale L., 1986, *A&A*, 157, 383
- Olgún-Iglesias A., Kotilainen J. K., León Tavares J., Chavushyan V., Añorve C., 2017, *MNRAS*, 467, 3712
- Olgún-Iglesias A., Kotilainen J., Chavushyan V., 2020, *MNRAS*, 492, 1450
- Orban de Xivry G., Davies R., Schartmann M., Komossa S., Marconi A., Hicks E., Engel H., et al., 2011, *MNRAS*, 417, 2721
- Osterbrock D. E., Pogge R. W., 1985, *ApJ*, 297, 166
- Paliya V. S., Rajput B., Stalin C. S., Pandey S. B., 2016, *ApJ*, 819, 121
- Pan H.-W., Yuan W., Yao S., Komossa S., Jin C., 2018, *ApJ*, 866, 69
- Page M. J., Symeonidis M., Vieira J. D., Altieri B., Amblard A., Arumugam V., Aussel H., et al., 2012, *Natur*, 485, 213
- Peng C. Y., Ho L. C., Impey C. D., Rix H.-W., 2011, *ascl.soft*
- Rakshit S., Stalin C. S., Chand H., Zhang X.-G., 2017, *ApJS*, 229, 39
- Romano P., Vercellone S., Foschini L., Tavecchio F., Landoni M., Knödseder J., 2018, *MNRAS*, 481, 5046
- Salucci P., Ratnam C., Monaco P., Danese L., 2000, *MNRAS*, 317, 488
- Sbarrato T., Dotti M., Ghirlanda G., Tavecchio F., 2018, *A&A*, 616, A43
- Schneider D. P., Fan X., Hall P. B., Jester S., Richards G. T., Stoughton C., Strauss M. A., et al., 2003, *AJ*, 126, 2579
- Shen Y., Richards G. T., Strauss M. A., Hall P. B., Schneider D. P., Snedden S., Bizyaev D., et al., 2011, *ApJS*, 194, 45
- Vestergaard M., 2004, *ASPC*, 311, 69
- Weinzirl T., Jooe S., Khochfar S., Burkert A., Kormendy J., 2009, *ApJ*, 696, 411
- Xu D., Komossa S., Zhou H., Lu H., Li C., Grupe D., Wang J., et al., 2012, *AJ*, 143, 83
- Yao S., Yuan W., Komossa S., Grupe D., Fuhrmann L., Liu B., 2015, *AJ*, 150, 23
- Yuan W., Zhou H. Y., Komossa S., Dong X. B., Wang T. G., Lu H. L., Bai J. M., 2008, *ApJ*, 685, 801
- Zhou H.-Y., Wang T.-G., Dong X.-B., Li C., Zhang X.-G., 2005, *ChJAA*, 5, 41
- Zhou H., Wang T., Yuan W., Lu H., Dong X., Wang J., Lu Y., 2006, *ApJS*, 166, 128
- Zhou H., Wang T., Yuan W., Shan H., Komossa S., Lu H., Liu Y., et al., 2007, *ApJL*, 658, L13

This paper has been typeset from a $\text{\TeX}/\text{\LaTeX}$ file prepared by the author.